RSC Advances

ROYAL SOCIETY OF CHEMISTRY

www.rsc.org/advances

RSC Advances

ARTICLE

Synergistic effects in mechanical properties of PLA/PCL blends with optimized composition, processing, and morphology

Received 00th January 20xx,
Accepted 00th January 20xx

DOI: 10.1039/x0xx00000x

www.rsc.org/

Aleksandra Ostafinska,[a] Ivan Fortelny,[a] Martina Nevoralova,[a] Jiri Hodan,[a] Jana Kredatusova[a] and Miroslav Slouf[a,*]

Abstract

Poly(lactic acid) (PLA) is a promising material for biomedical applications due to its biodegradability and high stiffness, but suffers from low toughness. We report that blending of PLA with another biodegradable polymer, poly(ε-caprolactone) (PCL), can increase the impact strength above the values of the individual components, while the other important macro- and micromechanical properties remain at well-acceptable level (above the theoretical predictions based on Equivalent Box Model). Although some previous studies indicated incompatibility of PLA and PCL polymers, we demonstrate that the melt-mixing of the polymers with optimized viscosities (PLA/PCL viscosity ratio ~ 1), the optimized composition (PLA/PCL = 80/20 by weight), and the optimal processing (compression molding with fast cooling) leads to optimal morphology (~0.6 μm particles of PCL in PLA matrix) and synergistic effect in the mechanical performance of the systems. In an additional set of experiments, we show that the addition of TiO_2 nanoparticles slightly improves stiffness, but significantly reduces the toughness of the resulting nanocomposites. The investigated systems were characterized by electron microscopy (SEM and TEM), notched impact strength, dynamic mechanical analysis, and microindentation hardness testing.

Keywords: biodegradable polymer blends, synergistic effects, impact strength, microindentation hardness testing

1. Introduction

Poly(lactic acid) (PLA) is one of the most promising polymers for biomedical applications due to its high modulus, perfect biocompatibility and full biodegradability. According to a recent review,[1] PLA is the most popular biopolymer for bone tissue engineering therapeutics, followed by poly(glycolic acid) (PGA), poly(lactic-co-glycolic) (PLGA), and poly(propylene fumarate) (PPF). In another review,[2] poly(lactides) and poly(glycolides) are mentioned as the most investigated biopolymers for orthopedic devices. PLA popularity stems from the fact that poly(L-lactide) (PLLA) has one of the highest elastic moduli among the biodegradable polymers (~2.7 GPa), which is less than the modulus of outer, cortical/compact bone (~20 GPa), but comparable to inner, cancellous/spongy bone (~0.1 GPa). Also Porter et al.[3] have mentioned aliphatic polyesters, such as PLA, PGA, poly(caprolactone) (PCL), and their copolymers, are the most commonly utilized polymers in a wide variety of clinical applications such as sutures, systemic drug delivery, coronary stents, fixation screws, etc.

However, application of neat PLA is strongly limited by its brittleness. Very efficient method of the improvement of toughness of brittle polymers is their blending with elastomers.[4] Good candidate for blending with PLA is biocompatible polyester PCL, which exhibits low glass transition temperature and high toughness. Indeed, PLA/PCL blends have been suggested and/or studied as a promising material for the controlled drug release,[5] the tissue engineering,[6] bone fixation devices,[7] and food packaging.[8] Nevertheless, the studies focused on the mechanical properties of the PLA/PCL blends have been rather contradictory. López-Rodríguez et al.[9] found strong decrease in strength at yield and at break and no increase in strain at break for PLA/PCL (80/20) blends in comparison with neat PLA. Such results are typical of incompatible polymers. Vilay et al.[10]

[a] Institute of Macromolecular Chemistry AS CR, Heyrovsky Sq. 2, 162 06 Prague 6, Czech Republic
* Corresponding author: slouf@imc.cas.cz

found moderate decrease in strength at yield and remarkable increase in strain at break with increasing content of PCL. Mittal et al.[11] concluded that PCL hinders crystallization of PLA due to some extent of intermixing of PCL and PLA phases. Fine but non-uniform morphology was observed in PLA/PCL (50/50) blends.[12] Bai et al.[13] studied dependence of the notched Izod impact strength on the size of PCL particles and crystallinity of PLA matrix in PLA/PCL (80/20) blends. They found that blends with crystalline PLA matrix achieved maximum impact strength for substantially smaller PCL particles than for blends with amorphous PLA matrix. Achieved maximum value of the strength for blends with crystalline PLA was about twice of the maximum value for blends with amorphous PLA. Recently, Urquijo et al.[14] found fine morphology and remarkable improvement in the elongation at break and impact strength of PLA/PCL blends; in this case the polymers seemed to have good interfacial adhesion.

Prevailing meaning in scientific community is that PLA and PCL are incompatible polymers and their blends should be compatibilized in order to achieve good mechanical properties.[15] A number of papers have been focused on compatibilization of PLA/PCL blends.[16-21] It was found that the addition of PCL-*b*-PLA diblock copolymer[16] and PLA-PCL-PLA triblock copolymers[16,18] led to finer morphology of PLA/PCL blends and enhanced their yield stress.[16] Maleic-anhydride-grafted PLA (PLA-*g*-PCL) was used as a reactive compatibilizer.[19] Addition of PLA-*g*-PCL decreased the size of PCL particles and enhanced elongation at break of PLA/PCL blends. Compatibilization of PLA/PCL blends with polyhedral oligomeric silsesquioxane (POSS) led to a decrease in PCL particle size in dependence on POSS functionalization or grafting with PCL-*b*-PLA. On the other hand, substantial positive effect of the compatibilization on maximum strength and elongation at break for PLA/PCL (70/30) was not detected.[17] Takayama et al.[21] found that the addition of lysine triisocyanate (LTI) to PLA/PCL blends reduced the immiscibility and thereby decreased the particle size of PCL. Furthermore, annealing of PLA/PCL/LTI blends increased the crystallinity, improved the bending modulus and strength as well.[21]

Recently, we have studied phase structure evolution in PLA/PCL blends with very similar viscosities of the components.[22] The blends exhibited particulate structure with quite small PCL particles up to 20 and 30 wt. % for compression molded and quenched samples, respectively. In well-defined, compression molded samples, the particles were slightly larger than in the quenched ones, but even the volume average of their radius was smaller than 1 μm till 20 wt. % of PCL. Moreover, PCL particles have been poorly visible in cryogenically fractured samples of PLA/PCL blends without etching, which indicated good interfacial adhesion. The combination of stiff PLA matrix with small, well-dispersed, toughening PCL particles was promising from the point of view of mechanical performance.

In this study, we optimized composition and processing of PLA/PCL blends so that we could obtain PLA/PCL blends fine particulate morphology and well-balanced combination of mechanical properties, namely stiffness and toughness, required for bone tissue engineering applications. Moreover, we prepared PLA/PCL/TiO_2 composites and investigated the effect of TiO_2 nanoparticles on morphology and mechanical performance. It is well known that TiO_2 nanoparticles have positive effect on tissue regeneration.[23] TiO_2 nanoparticles were also reported to influence crystallization kinetics, crystallinity, melting point and glass transition of polymers.[24,25] Nakayama at al.[26] showed that addition of TiO_2 nanoparticles into PLA matrix lead to the photodegraded product in comparison with pure PLA. Therefore, the structure, thermal and mechanical properties of PLA/PCL/TiO_2 nanocomposites besides neat PLA/PCL blends were the second object of this study. Last but not the least, we characterized the blends and composites also by microindentation hardness testing and investigated the relationship among morphology, micromechanical properties, macromechanical properties and predictive theory based on equivalent box model.[27]

2. Experimental

2.1 Materials

Two biodegradable polymers: polycaprolactone (PCL; Capa 6800; The Perstorp Group; Sweden; T_m = 60 °C) and polylactide (PLA; Ingeo 4032D; NatureWorks LLC, USA; T_m = 166 °C) were used in this study. The polymers were selected so that the PLA/PCL viscosity ratio was ~1 (see section 2.2 and Fig. 1). A commercial titanium dioxide (TiO_2; anatase, particle size 50 – 200 nm) was supplied by Sigma-Aldrich, USA. Tetrahydrofuran (THF; Lachner, Czech Republic) was used as an etching substance of PCL phase.

2.2 Rheological characterization of blend components

Rheological properties of pure PLA and PCL were determined using a Physica MCR 501 rheometer (Anton Paar, Austria) equipped with a convection temperature device CTD 450 and parallel plate fixture of 25 mm diameter. The samples were measured in dynamic mode at a temperature of 180 °C. The experiments were performed at a strain 5% in the linear viscoelasticity region, confirmed from strain sweep tests at the frequency 1 Hz. Frequency sweep for both polymers is shown in Fig. 1.

2.3 Blend preparation

All samples, i.e. pure PLA and PCL, PLA/PCL blends and PLA/PCL/TiO_2 composites (Table 1) were prepared by melt mixing (PCL at 120°C, PLA and blends at 180 °C and 60 rpm, 10 min) inside the chamber B 50 EHT of a Brabender Plasticorder (Brabender, Germany). Before mixing the neat polymers were dried in vacuum oven (PCL: 40 °C for 12 h; PLA 80 °C for 4 h). For PLA/PCL systems, the samples with compositions 90/10, 85/15, 80/20, 75/25, 70/30, 60/40, and 50/50 were prepared. The PLA/PCL (80/20) blends with 10 wt.% of TiO_2 (PLA/PCL/TiO_2 = 72/18/10 wt.%) were prepared in three ways (see also Table 1): (i) all components were premixed in a beaker and added together into the melt-mixing chamber – the composite denoted as 72/18/10/a, (ii) the TiO_2 particles

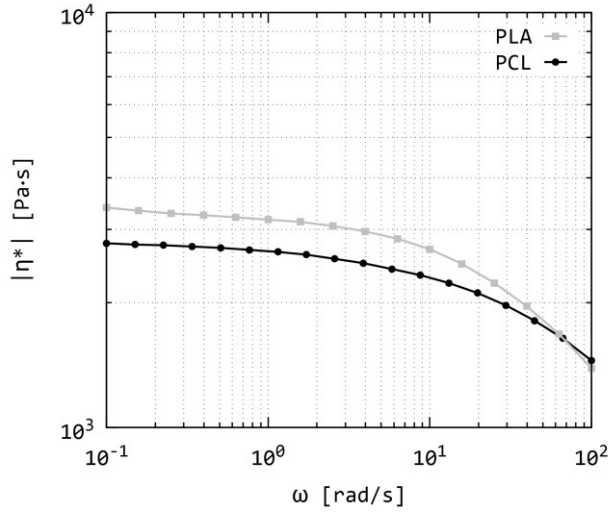

Fig. 1 The absolute value of complex shear viscosity at 180 °C as a function of angular frequency of PLA and PCL biopolymers.

Table 1. Summary of the composition and preparation of all PLA/PCL/TiO_2 composites.

Sample	PLA (%)	PCL (%)	TiO_2 (%)	Preparation
76/19/5/a	76	19	5	all components mixed together
72/18/10/a	72	18	10	all components mixed together
72/18/10/b	72	18	10	from masterbatch of PLA with TiO_2
72/18/10/c	72	18	10	from masterbatch of PCL with TiO_2

were mixed with PLA as a masterbatch and then blended with PCL – the composite denoted as 72/18/10/b, and (iii) the TiO_2 particles were mixed with PCL as a masterbatch and then blended with PLA – the composite denoted as 72/18/10/c. The composited with 5 wt. % of TiO_2 (PLA/PCL/TiO_2 = 76/19/5/a) was prepared only in the first way, i.e. by mixing all three components together (Table 1). All melt-mixed samples were compression molded by two hydraulic presses (Fontijne Grotnes, Netherlands; the first press: 180 °C, 2 min at 50kN + another 8 min at 220 kN, then moved to the second press: 60 °C, 2 min. at 220 kN + subsequent cooling with water for 15 min to reach the ambient temperature). The resulting samples (4 mm x 10 mm x 85 mm specimens) were used for further characterization by microscopy, Charpy notched-impact test, DMA, DSC, and microindentation hardness testing, as described below.

2.4 Scanning electron microscopy (SEM)

The morphology of PLA/PCL blends and PLA/PCL/TiO_2 composites was visualized by means of scanning electron microscopy (SEM) and the average particle size was quantified by an image analysis of the resulting SEM micrographs as described in our previous studies.[22,28] The micrographs were obtained with a microscope Quanta 200 FEG (FEI, USA) using a secondary electron imaging (SEM/SE) and backscattered electron imaging (SEM/BSE) at 5 and 10 kV, respectively. The PLA/PCL blends were smoothed under liquid nitrogen[29] and then etched (tetrahydrofuran vapor at 45°C for 4 min) in order to visualize the phase structure (tetrahydrofuran vapors etched PCL particles faster than PLA matrix). The PLA/PCL/TiO_2 composites were broken in liquid nitrogen (i.e. below their glass transition temperature) in order to visualize TiO_2 particles dispersion in the polymer matrix. Before observation in the electron microscope, the samples were fixed on a metallic support with conductive silver paste (Leitsilber G302, Christine Groepl, Austria) and sputtered with Pt (vacuum sputter coater, SCD 050, Balzers, Lichtenstein) in order to minimize charging and sample damage.

2.5 Transmission electron microscopy (TEM)

Detailed morphology of PLA/PCL/TiO_2 composites was studied by transmission electron microscopy (TEM). The micrographs were obtained with a TEM microscope Tecnai G2 Spirit Twin (FEI, Czech Republic). The specimens for TEM investigation were prepared by ultramicrotomy (room temperature, cutting speed 20mm/s, section size ca. 300×300 µm, and section thickness 50 nm; the ultrathin sections were left floating on water and collected on copper grids). The resulting ultrathin sections were observed in the TEM microscope using bright field imaging at 120 kV.

2.6 Differential scanning calorimetry (DSC)

The thermal properties of the samples were studied using a DSC Q2000 instrument (TA Instruments) with nitrogen purge flow 50 cm^3/min. The instrument was calibrated for temperature and heat flow using indium as a standard. Samples of about 5 mg were encapsulated into aluminium pans. The analyses were performed in cycle heating – cooling – heating from -20 °C to 200 °C at 10 °C/min. Melting points, T_m, were determined from the position of the melting peak maximum. Crystallinity of PCL particles were calculated as the area under the melting peak normalized to 100 % crystalline PCL (136 J/g).[30] Crystallinity of PLA matrix (X_c(PLA)) was calculated according to the following formula, which takes into account cold crystallization of the polymer:

$$X_C(\mathrm{PLA}) = [\,|\Delta H_m(\mathrm{PLA})| - |\Delta H_{cc}(\mathrm{PLA})|\,] / \Delta H_m^0(\mathrm{PLA}) \times 100\%/w(\mathrm{PLA}) \quad (1)$$

where ΔH_m(PLA) is the enthalpy of the PLA melting peak, ΔH_{cc}(PLA) is the enthalpy of the PLA cold crystallization peak, ΔH_m^0(PLA) is the melting enthalpy of 100 % crystalline PLA (93.6 J/g).[31]

2.7 Charpy notched-impact test

Charpy notched-impact strength was measured on a non-instrumented impact pendulum (Ceast Resil Impactor Junior - Ceast S.p.A., Italy) with nominal energy 4 J and support span 62 mm, according to standard ISO 179-1 at room temperature. Testing specimens corresponded to the ISO 179-1/1 type (length 80 mm; width 10 mm; thickness 4 mm) and were prepared by compression molding (at least six specimens per sample) as described in section 2.3. The notches (A type), with

depth of 2 mm and a tip radius of 0.25 mm, were prepared with a V-knife. Impact blow was in the edgewise direction of the test specimens.

2.8 Dynamic mechanical analysis (DMA)

Mechanical properties of PLA, PCL, PLA/PCL blends and PLA/PCL/TiO_2 composites were tested by dynamic-mechanical analysis (DMA) at room temperature. The absolute values of complex moduli $|G^*|$ – were measured in the rectangular torsion using a Physica MCR 501 rheometer (Anton Paar GmbH, Austria). The experiments were performed at a strain 0.1% in the linear viscoelasticity region, confirmed from strain sweep tests at the frequency 1 Hz. The measurements were carried out in the frequency range 10^{-1}–10^{2} rad/s and the results from at least three specimens per sample were averaged. The specimens (25×10×4 mm) were stored in a desiccator.

2.9 Micromechanical properties

Micromechanical properties were characterized by instrumented microindentation hardness tester (Micro-Combi Tester; CSM Instruments, Switzerland). Smooth cut surfaces for the microindentation experiments were prepared from compression molded plates (thickness 4 mm) that were cut perpendicularly with a rotary microtome (RM 2155; Leica, Austria) using a freshly broken glass knife (Knifemaker 7800; LKB Bromma, Sweden). For each specimen, at least two independent smooth surfaces were prepared, and at least 10 indentations were carried out per surface, i.e. each sample was measured at least 20×, and the results were averaged. All indentations were performed with Vickers indenter (diamond square pyramid, angle between two non-adjacent faces 136°; details about experiment geometry have been described elsewhere);[32,33] the indenter was forced against the polymer surface with the following parameters: load 1.962 N (200 gf), load time 6 s, and loading/unloading rate 0.417 N/s (25,000 mN/min). For given materials and experimental setup, the size of the indents on the polymer surface was >100 μm, i.e. well above the coarseness of the phase structure. Consequently, the microindentation experiments yielded overall/non-local information about the properties of investigated systems, which could be compared with macroscopic measurements. The curves showing applied force (F) vs. penetration depth (h) were used to calculate indentation hardness (H_{IT}) and indentation modulus (E_{IT}) using software Indentation 5.18 (CSM Instruments, Switzerland) according to theory of Oliver and Pharr.[34]

2.10 Comparison of macro- and micromechanical properties with predictive models

Physical properties, such as elastic modulus and yield strength, of the polymer blends with particulate, fibrous and partially co-continuous structures can be predicted by various models. For elastic modulus, the simplest model is rule-of-mixing (RoM; also known as additivity rule or linear model):

$$E_b = E_1 v_1 + E_2 v_2, \quad (2)$$

where E_b is the elastic modulus of the blend, and E_1, E_2, v_1 and v_2 are the elastic moduli and volume fractions of the components. The Eq. 2 represents the upper limit for E_b of immiscible blends, corresponding to the ideal case of composite/blend with very long fibers ($L \gg d$, where L and d are fiber length and diameter, respectively). In our case of polymer blends with particulate and/or partially co-continuous structures, more realistic prediction of E_b can be obtained with Equivalent Box model (EBM),[27] whose final equation for elastic modulus reads:

$$E_b = E_1 v_{1p} + E_2 v_{2p} + v_s^2/[(v_{1s}/E_1) + (v_{2s}/E_2)], \quad (3)$$

where v_{ij} are volume fractions, in which the subscript i represents the first (i = 1) or the second (i = 2) component, while the subscript j denotes the parallel (j = p) or serial (j = s) branch of the EBM model. The parallel and serial branch of the EBM model correspond to the volume fractions that exhibit particulate and co-continuous morphology, respectively. The volume fractions v_{ij} can be either estimated using percolation theory, or determined experimentally from electron micrographs, as described elsewhere.[27,35,36] Due to the proportionality among elastic moduli from standard tensile tests (E_b), absolute values of complex shear moduli from DMA measurements ($|G^*|$; section 2.8), and indentation moduli from microindentation experiments (E_{IT}; section 2.9):

$$E \propto |G^*| \propto E_{IT} \quad (4)$$

the predictive models (Eq. 2 and 3) can be applied also on moduli from DMA and microindentation experiments. Analogously to Eq. 2 and 3, also the upper limit of yield stress of a polymer blend (σ_{Yb}) can be estimated from RoM (Eq. 5) and more realistic estimate of σ_{Yb} can be obtained from EBM model (Eq. 6):

$$\sigma_{Yb} = \sigma_1 v_1 + \sigma_2 v_2 \quad (5)$$

$$\sigma_{Yb} = \sigma_{Y1} v_{1p} + \sigma_{Y2} v_{2p} + A\sigma_{Y1} v_s \quad (6)$$

where $\sigma_{Y1} < \sigma_{Y2}$, the meaning of volume fractions (v_{ij}) is the same as described above (Eq. 2), v_s is the sum of v_{1s} and v_{2s}, and parameter $A \in \langle 0; 1 \rangle$ describes the extent of interfacial debonding. Two limiting values of σ_{Yb} can be distinguished by means of Eq. 6: the interfacial adhesion is so weak that complete debonding occurs before yielding between the fractions of constituents coupled in series (A = 0); (ii) the interfacial adhesion is strong enough to transmit the acting stress between constituents so that no debonding appears in the course of yielding (A = 1).[27,35,36] Again, the predictive models (Eq. 4 and 5) can be applied also on the results of microindentation hardness testing, i.e. on the values of indentation hardness (H_{IT}), which are connected with the yield stress by Tabor relation:[37]

$$H_{IT} \approx 3\sigma_Y; \quad (7)$$

the sign ≈ in Eq. 7 means that the Tabor relation was developed and justified for plastic materials, while for viscoelastic materials, such as polymers, it is accepted as the first approximation.[32]

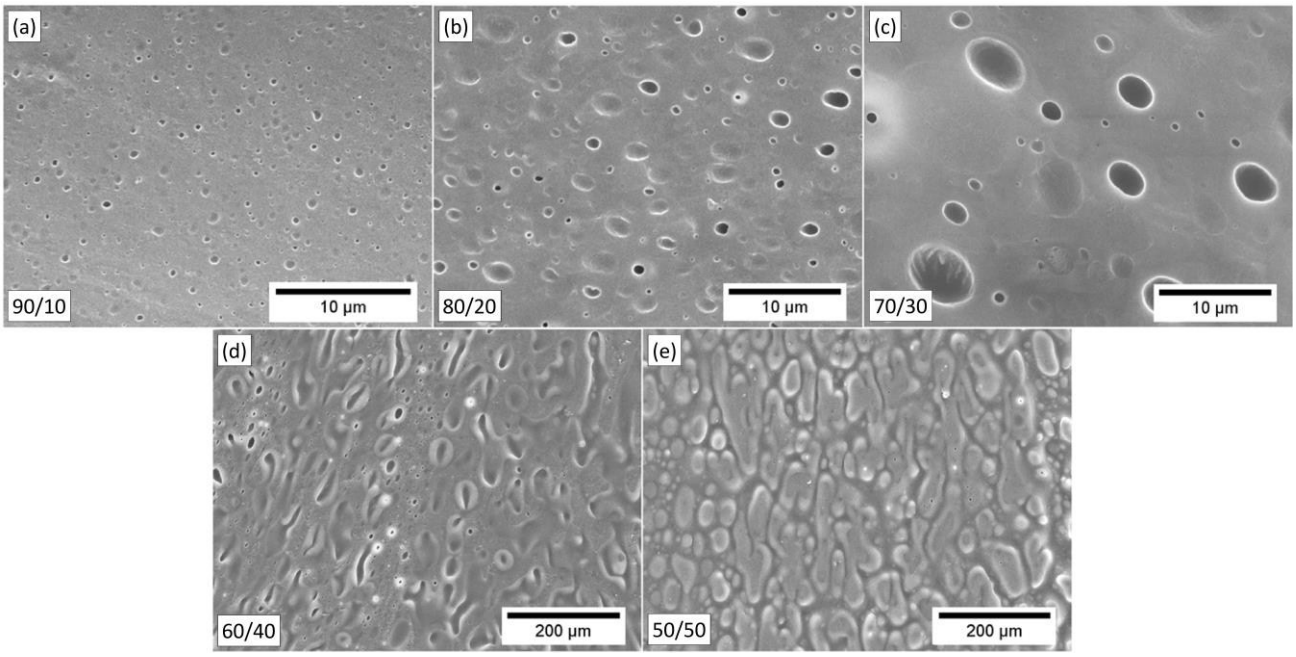

Fig. 2 SEM/SE micrographs of smoothed and etched compression molded samples of PLA/PCL blends.

Table 2. Morphological parameters of the PLA/PCL blends with particulate structure.

PLA/PCL	µ(N) (µm)	σ(N) (µm)	µ(V) (µm)	σ(V) (µm)
90/10	0.30	0.17	0.58	0.24
85/15	0.56	0.29	0.97	0.33
80/20	0.58	0.38	1.34	0.54
75/25	0.72	0.74	3.29	1.88
70/30	0.83	0.96	6.96	4.00

µ(N) and σ(N) arithmetic mean and width of number distribution of particle size. µ(V) and σ(V) = arithmetic mean and width of volume distribution of particle size. The values of µ(N), σ(N), µ(V) and σ(V) were calculated with program MDISTR.[28]

3. Results and discussion

3.1 PLA/PCL blends

3.1.1 Morphology of PLA/PCL blends

Phase morphology of the PLA/PCL blends is shown in Fig. 2 and quantified in Table 2. For PCL content up to 20-25 wt. % (Fig. 2a, b), the blends exhibited a fine phase structure with small particles and narrow particle size distribution. At 30 wt. % (Fig. 2c) the phase structure coarsened and the particle size distribution broadened, as evidenced also by the values of distribution width given in Table 2. For PCL content ≥40 wt. % the phase morphology turned to co-continuous (Fig. 2d, e).

As both PCL and PLA are semicrystalline polymers, their crystallinity (w_c) and lamellar thickness (l_c) could have an impact on their mechanical properties.[33,35,38] These morphological parameters were assessed from DSC in the form of DSC crystallinities ($X_c \sim w_c$) and melting points ($T_m \sim l_c$). As for the minority phase, PCL, the melting points (varying around 62 °C) and crystallinities (varying around 55 %) did not show any apparent trend, which suggested that given preparation procedure did not influence PCL supermolecular structure. For PLA matrix (Table 3) we observed cold crystallization around 98 °C and melting of the crystalline phase around 168 °C. The cold crystallization evidenced that the cooling process was quite fast and, as a result, the final crystallinity values of PLA matrix (calculated according to Eq. 1) were quite low.

It is worth reminding that the fine phase structure of the PLA/PCL blends with particulate structure (up to composition 75/25 wt. %) was achieved intentionally and in accord with theoretical predictions. In order to obtain small PCL particles in PLA matrix, we optimized the composition and preparation as follows: Firstly, we selected the components with similar viscosities (section 2.2; Fig. 1), which led to the fine phase morphology.[22] Secondly, we optimized the compression molding procedure with the aim to avoid frozen stresses and simultaneously to minimize particle coalescence and subsequent coarsening of phase structure. The fine particulate morphology of PCL was expected to result in the highest toughening of PLA matrix.[4,39] As the increase of PLA stiffness with crystallinity is quite moderate (less than 15 % if the crystallinity is increased from 9 to 70%),[40] we sacrificed the crystallinity and slightly higher stiffness in favor of fine phase morphology and strongly improved toughness.

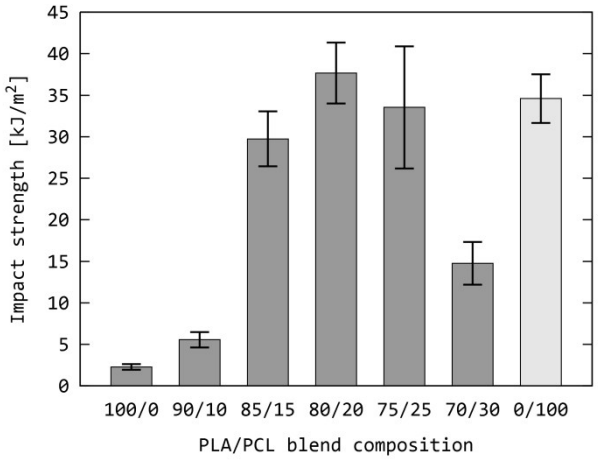

Fig. 3 Notched impact strength of PLA/PCL blends; the error bars represent standard deviations.

Table 3. Thermal parameters of PLA/PCL and PLA/PCL/TiO2 systems obtained by DSC.

Composition of PLA/PCL/TiO_2	$T_{cc,PLA}$ (°C)	$\Delta H_{cc,PLA}$ (J/g)	$T_{m,PLA}$ (°C)	$\Delta H_{m,PLA}$ (J/g)	$X_{c,PLA}$ (%)
100/0	106.0	-22.2	168.2	31.2	9.7
90/10	92.2	-19.3	167.4	27.2	9.5
80/20	94.4	-19.0	170.1	24.4	7.2
70/30	97.2	-18.0	170.2	22.1	6.4
76/19/5/a	96.7	-19.3	168.3	24.2	7.0
72/18/10/a	97.6	-19.4	166.9	24.0	6.9
72/18/10/b	94.5	-17.6	167.7	24.3	10.0
72/18/10/c	99.2	-18.2	167.6	22.9	7.1

$T_{cc,PLA}$ = temperature of cold crystallization, $\Delta H_{cc,PLA}$ = enthalpy of cold crystallization, $T_{m,PLA}$ = melting temperature, $\Delta H_{cc,PLA}$ = melting enthalpy, $X_{c,PLA}$ = degree of crystallinity.

3.1.2 Macromechanical properties of PLA/PCL blends

The main objective of this work was to improve PLA toughness by means of PCL. The toughness was measured in the form of notched impact strength (Fig. 3). We measured only the blends with particulate structure (i.e. up to composition 70/30), in which the PCL particles were expected to act as an impact modifier. According to our expectations and available literature, the pure PLA was very brittle (impact energy < 2.5 kJ/m^2). The impact strength of PLA/PCL blends steeply increased with PCL content, reaching a maximum at 80/20 composition.

The toughness of 80/20 blend exceeded even the toughness of pure PCL impact modifier, which meant that there was a synergistic effect. Moreover, the impact energy of 80/20 blend was more than 16 times higher in comparison with pure PLA. This was well above the increase reported in analogous studies. For example, Odent et al.[41] used 10% of random aliphatic copolyesters as impact modifiers for PLA (impact energy of pure PLA ~2.5 kJ/m^2 like in this work) and increased the impact strength ca 3 times (the best impact energy achieved ~7.1 kJ/m^2). In another recent study of Urquijo et al.[14] the improvement of the impact strength of the PLA/PCL blend (80/20) was ca twofold, slightly increasing for higher concentrations of PCL. Therefore, it seems that our strong, synergistic improvement of PLA toughness could be attributed partially to the optimized composition, preparation and morphology of the blends, and partially to serendipity when combining all favorable effects together.

Recent analysis[42] pointed out that the notched impact strength of polymer blends is a complex function of multiple factors, the most important of which are particle diameter, D, volume fraction of the dispersed phase, φ, and particle-matrix adhesion. Both theoretical analyses and experimental studies of the fracture process in rubber-toughened polymers[4,42-44] showed that the brittle-ductile (BD) and ductile-brittle (DB) transitions could be observed for impact strength as a function of D. BD transition occurs when the blend contains particles above a critical minimum size that initiate cavitation, while DB transition is associated with crazes initiated at bigger particles. Therefore, high impact strength for a combination of polymers with given φ can be achieved only for the droplet diameters between BD and DB transitions. An increase in the impact strength with D near BD transition is frequently very steep (cf. Fig. 25.16 in ref.[44]), whereas the related decrease near DB transition is usually slower. Experimental studies rubber-toughened thermoplastics showed that the optimal D is higher for brittle amorphous thermoplastics (such as PS and PMMA; optimal D ~ 1 μm) than for semicrystalline thermoplastics (such as PP and PA; optimal D ~ 0.2–0.3 μm). As the above mentioned semicrystalline thermoplastics exhibit substantially higher ductility in comparison with the amorphous ones, it not quite clear if matrix crystallinity or its toughness has more decisive effect on optimal value of D. The optimal D for PLA/PCL blends was studied by Bai et al.[13] who found that it is larger for blends with the amorphous PLA matrix than with the semicrystalline one. They obtained twice larger notched Izod impact strength for optimum PCL particle size in PLA/PCL blend with semicrystalline matrix in comparison to the blend with the amorphous matrix. The optimum weight-average diameter for PLA/PCL (80/20) blends with a low crystallinity of PLA obtained by Bai et al.[13] (0.86 μm) is in between number-average and volume-average D for our system with the same composition (see Table 2). This is in agreement with the fact that our combination of PLA and PCL grades with the method of the blend preparation led to optimum morphology and toughness of our PLA/PCL blend with composition 80/20. For higher concentrations of PCL (Fig. 3, compositions 75/25 and 70/30) the average D was strongly increased (Table 2) and evidently exceeded the optimal value for our system. For lower concentrations of PCL (Fig. 3, compositions 85/10 and 90/10) the decrease in D below the optimal value (Table 2) combined with decreasing amount of rubber phase with the toughening effect[44] resulted in observed steep decrease in the impact strength.

The stiffness of PLA/PCL blends was assessed in the form of absolute values of complex moduli, $|G^*|$, at angular frequency 1 rad/s from DMA measurements (Fig. 4, black squares). As expected, the addition of soft PCL component into PLA matrix

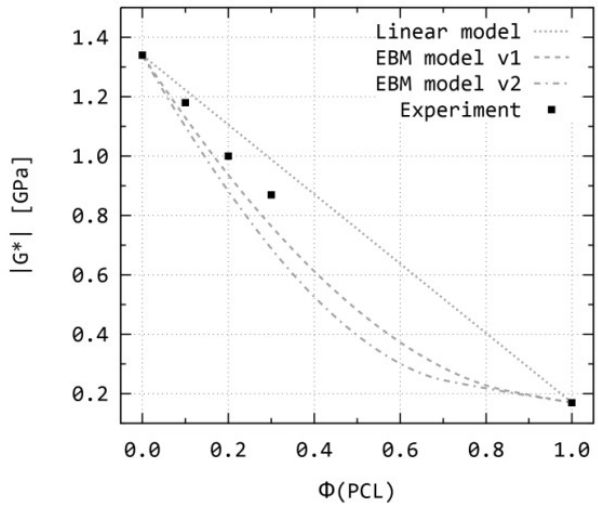

Fig. 4. Absolute values of the complex shear moduli |G*| from DMA experiments (black squares) and their comparison with predictive models: linear model/rule of mixtures (dotted line), EBM model with default parameters (dashed line), and EBM model with co-continuity parameter adjusted according to SEM micrographs (dash-and-dot line).

decreased the final modulus of the PLA/PCL blends. This represented an obvious penalty for toughening of brittle polymers with elastomers.[4] However, the decrease in $|G^*|$was not dramatic: It was lower than predicted by EBM model (Eq. 3) with both default (Fig. 4, dashed line) and morphology-adjusted parameters (Fig. 4, dash-and-dot line). The adjustment of the EBM parameters consisted in changing the value of volume fraction, at which the blend morphology changes from particulate to co-continuous (Eq. 3; refs.[27,35]): the default value based on the percolation theory (0.16) was changed to more realistic value based on SEM micrographs (0.35; Fig. 2). More detailed explanation about usage/adjusting EBM model parameters can be found in section 2.10 and references therein. In any case, the experimental moduli were above both EBM predictions. Therefore, we conclude that PLA/PCL (80/20) blend offers a combination of an excellent toughness and well acceptable stiffness.

Macromechanical properties (Figs. 3 and 4) demonstrated that PLA/PCL blends under study did not behave as incompatible systems. This was in agreement with conclusions of Urquijo et al.[14] The results documented that the interfacial adhesion between PLA and PCL is sufficient for achievement of the high impact strength if blends with optimum size of the PCL particles are prepared. Insufficient enhancement of the impact strength of PLA with the addition of PCL found in some studies[9,14,41] was apparently caused by an improper size of the PCL particles, as explained above, in the second paragraph in this section. Moreover, the recent study of Bai et al.[13] suggested that even higher increase in the impact strength could have been achieved for the system PLA/PCL systems with higher crystallinity of the matrix, on condition that the morphology would be optimized.

It has been shown that crystallization of PLA leads to a change in the toughening mechanism in PLA blends from crazing to shear-yielding.[41,45,46] It is generally supposed that shear-yielding causes dissipation of more energy prior to fracture with respect to crazing. We confirmed that the interrelation among the composition of PLA/PCL blends, the size of PCL particles and the crystallinity of PLA matrix are quite complex and that they should be an object of further studies.

3.1.3 Micromechanical properties of PLA/PCL blends

Microindentation hardness testing was employed to supplement and verify the DMA experiments and EBM predictions (Fig. 4). The microindentation experiments yielded the values of indentation modulus, E_{IT}, and indentation hardness, H_{IT}. The indentation moduli, E_{IT}, from micromechanical measurements slowly decreased with the increasing PCL concentration, analogously to the absolute values of shear moduli $|G^*|$ from DMA measurements. The correlation between microscopic and macroscopic moduli is illustrated in Fig. 5. We note that the theoretical linear relationship between tensile elastic and shear modulus (Eq. 8, ref.[47]),

$$E = 2G(1+\nu) \qquad (8)$$

holds very well (E = tensile elastic modulus ~ E_{IT}, G = shear modulus ~ $|G^*|$, and ν = Poisson's ratio). If we take a common value of Poison's ratio for semicrystalline polymers: ν ≈ 0.45,[48] the theoretical slope in the E-G graph should be ≈2.9 and the experimental value was 2.98 ± 0.06. Moreover, Eq. 8 suggests that the intercept in the graph should be zero and the experimental value was 0.12 ± 0.06. The fact that both the slope and the intercept corresponded quite well to the theoretical values confirmed the correctness of our measurements. It is worth noting that the good agreement of the experimental values with Eq. 8 resulted from the suitable selection of measurement conditions: the same measurement temperatures and similar time scales (in our case, we used values of $|G^*|$ at ω = 1 rad/s and values of E_{IT} after loading time 6 s as recommended by Calleja et al.[32]).

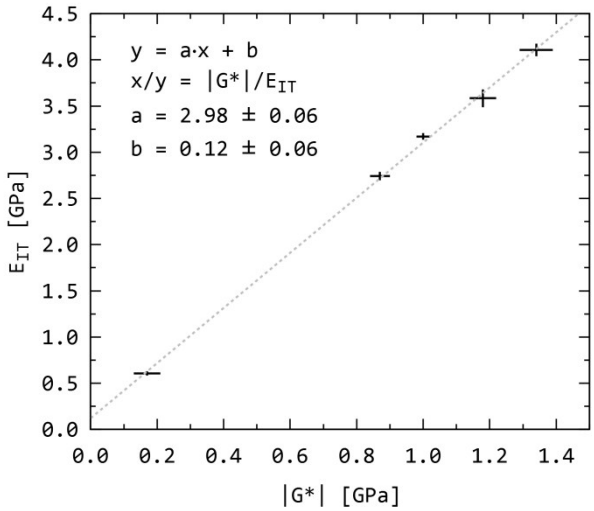

Fig. 5. Correlation between macroscopic modulus, $|G^*|$, from DMA measurements and microscopic indentation modulus, E_{IT}, from microindentation hardness testing.

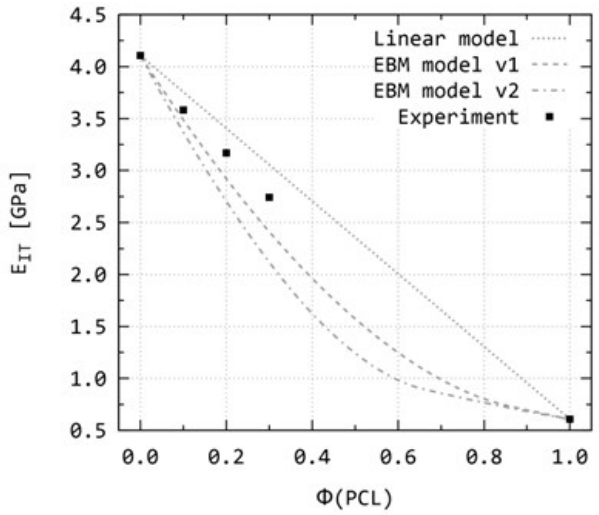

Fig. 6. Microindentation modulus, E_{IT}, compared with predictive models: dotted line – linear model, dashed line – EBM model with default parameters, and dash-and-dot line – EBM model with co-continuity parameter adjusted according to SEM micrographs. Description of models is given in section 2.9 and references therein.

The experimental values of micromechanical properties (E_{IT} and H_{IT}) were also compared with theoretical predictions based on EBM (Eq. 3 and 6; Fig. 6 and 7). Although the EBM model has been developed for macroscopic properties, it can be applied to microscopic properties as well (Section 2.9; ref.[35]). Figures 6 and 7 show experimental values of E_{IT} and H_{IT} as functions of the blend composition, compared with various models like in Fig. 4: (i) simple linear model (dotted line), (ii) EBM model with default parameters (dashed line; the model is based on the assumption that partial continuity of minority phase occurs at volume fraction ≈ 0.16 – this assumption derives from percolation theory),[27] and (iii) EBM model with parameters adjusted according to real morphology of our blends (dash-and-dot lines; the model calculated with PCL continuity starting at volume fraction ≈0.35 – this value was estimated from SEM micrographs in Fig. 2; the other parameters of the EBM model were left at their default values).[27,35,36]

The indentation moduli E_{IT} (Fig. 6) were below the ideal case represented by linear model (Eq. 2), but above the more realistic prediction based on EBM models (Eq. 3). In other words, the decrease in micromechanical properties caused by PCL was not critical, having been even better than theoretical predictions. This was in excellent agreement with the results for the shear moduli from DMA measurement $|G^*|$ (compare Figs. 4 and 6), confirming not only the reliability of our results, but also the better-than-expected stiffness of the resulting PLA/PCL blends.

The experimental H_{IT} values were even above the linear model for the low PCL concentrations (Eq. 5), and safely above EBM predictions (Eq. 6) for all compositions (Fig. 7), even when the EBM curves were calculated for maximal interfacial adhesion (EBM debonding parameter at its maximum value A = 1, see section 2.9). This behavior, i.e. positive deviations of elastic modulus (which is proportional to E_{IT} according to Eq. 4) and yield strength (which is proportional to H_{IT} according to Eq. 7) is typical of compatible and partially miscible blends. Such blends form strong interfacial layer with improved properties and frequently exhibit synergistic effects.[35,49] We conclude that microindentation experiments confirmed good interfacial adhesion and synergistic effects that were observed at macroscopic scale (Figs. 3 and 4).

3.2 PLA/PCL/TiO_2 composites

3.2.1 Morphology of PLA/PCL/TiO_2 composites

For the PLA/PCL (80/20) blend, we investigated also the effect of addition of TiO_2 nanoparticles. Four different PLA/PCL/TiO_2 composites with PLA/PCL ratio (4/1) were prepared (Table 1). The ratio (4/1) was selected because the PLA/PCL (80/20) blend exhibited the best combination of properties: the fine morphology (Fig. 2), the highest toughness (Fig. 3), and the sufficient stiffness (Fig. 4). According to available literature, TiO_2 nanoparticles might influence PLA/PCL crystalline structure (crystallization kinetics, crystallinity, and lamellar thickness), PLA/PCL phase morphology, physical properties (modulus, thermal stability), modify the compatibility of the polymer components (localization at the interphase) and even improve tissue regeneration.[23-25,50]

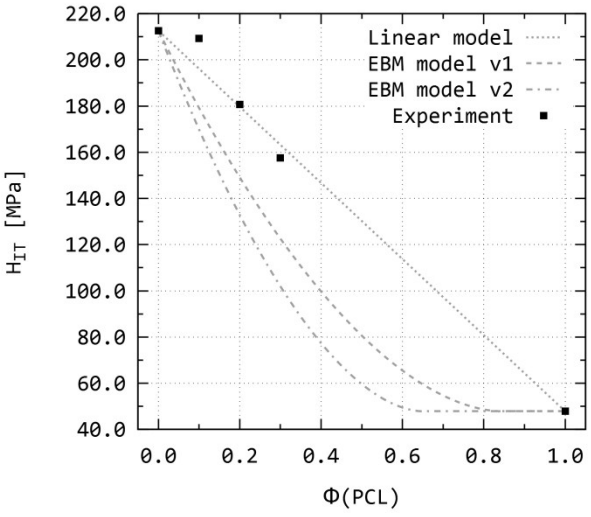

Fig. 7. Microindentation hardness, H_{IT}, compared with predictive models: dotted line – linear model, dashed line – EBM model with default parameters, and dash-and-dot line – EBM model with co-continuity parameter adjusted according to SEM micrographs. Description of models is given in section 2.9 and references therein.

RSC Advances

ARTICLE

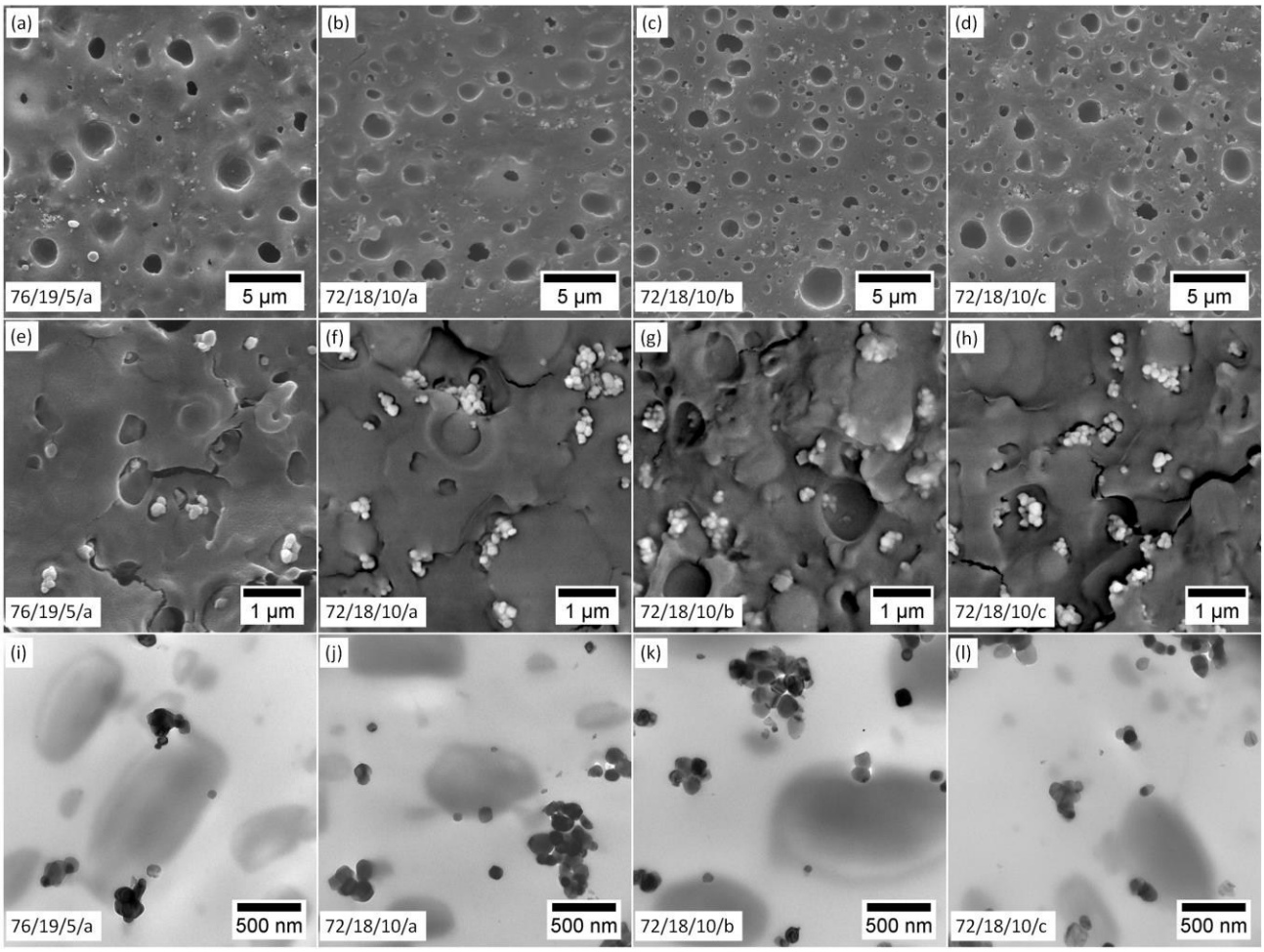

Fig. 8. Morphology of PLA/PCL/TiO_2 composites; description of the composites is given in Table 1. (a–d) SEM/SE micrographs of smoothed and etched surfaces, (e–h) SEM/BSE micrographs of fracture surfaces and (i–l) TEM micrographs of ultrathin sections.

Morphology of the prepared blends is summarized in Fig. 8. SEM micrographs of smoothed and etched surfaces (Fig. 8a–d) evidenced that the addition of TiO_2 particles had negligible effect on the size distribution of PCL particles. SEM micrographs of fracture surfaces prepared under liquid nitrogen (Fig. 8e–h) indicated that interfacial adhesion between PLA and PCL is quite strong (fracture frequently propagated through the particles instead along the interface) and that the TiO_2 nanoparticles tend to form agglomerates regardless of preparation procedure (the preparation procedures are listed in Table 1). TEM micrographs of ultrathin sections (Fig. 8i–l) showed the dispersion of TiO_2 nanoparticles between PLA and PCL components in higher detail: the nanoparticles were localized partly in PLA matrix, partly on the PLA/PCL interface and just occasionally in PCL inclusions. This suggested why the addition of TiO_2 nanoparticles had little effect on the size distribution of PCL inclusions: Nanofillers can affect the morphology of polymer blends through the change of the viscosity ratio of the dispersed phase and matrix or by direct suppression of droplet coalescence due to their localization at the interface. In our case, the particles localized at the interface did not cover the surface of PCL particles completely and, as a result, they were inefficient at the coalescence suppression. A small amount of TiO_2 dispersed in PLA and PCL probably did not change viscosity ratio of the blend components remarkably and so their effect on the blend morphology was almost negligible. The TiO_2 nanoparticles also tended to form small agglomerates, but their size did not

exceed 1 µm. This PLA/PCL/TiO_2 morphology was similar to that observed by Mofokeng et al.,[50] where the most of TiO_2 nanoparticles was dispersed in PLA matrix, but the size of nanoparticle agglomerates was in micrometer range. Somewhat better dispersion observed in our work might be attributed to slightly different melt-mixing conditions and smaller nanoparticle size in the above mentioned study.[50] From the microscopic point of view, it is interesting that the PLA matrix (light-gray background) was quite easily distinguished from PCL particles (dark-gray spheres and elipses), although the microscopic specimens were not stained and the accelerating voltage was as high as 120 kV. The observed contrast could be attributed to somewhat different densities of the two polymers (PCL = 0.98 g/cm^3 and PLA = 1.12 g/cm^3) and to the high sensitivity of modern digital cameras for TEM microscopes (in our case 11MPix CCD camera Morada; Olympus).

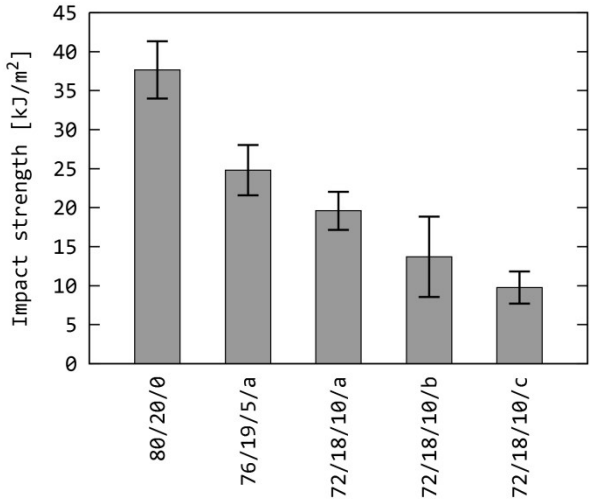

Fig. 9. Charpy impact strength of PLA/PCL/TiO_2 composites; description of the composites is given in Table 1.

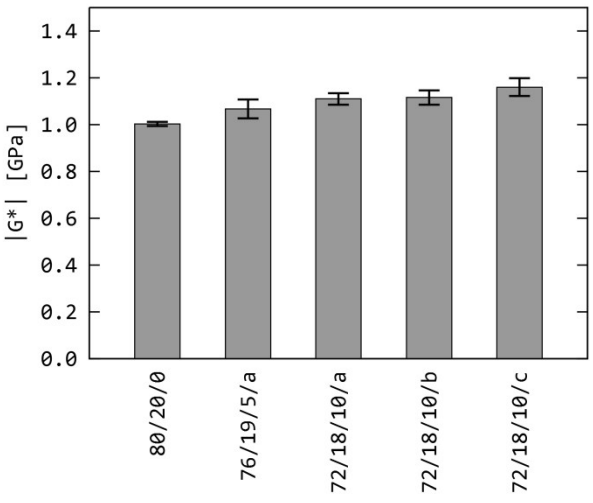

Fig. 10. Absolute values of complex modulus of PLA/PCL/TiO_2 composites; the values were taken from DMA measurements at ω = 1 rad/s; description of the composites is given in Table 1.

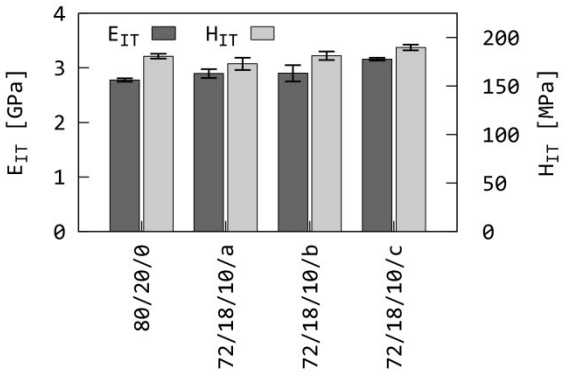

Fig. 11. Indentation modulus (E_{IT}) and indentation hardness (H_{IT}) of PLA/PCL/TiO composites obtained from microindentation hardness testing; the composites are described in Table 1.

The crystallinity of PLA in all composites was measured as well. The results are collected in Table 3. The addition of TiO_2 particles did not change the crystallinity of PLA matrix, which was similar as for pure PLA (~10%). The crystallinity of PCL inclusions (~ 55 %) was not changed either.

3.2.2 Macromechanical properties of PLA/PCL/TiO_2 composites

As we mentioned above, the morphology of PLA/PCL (80/20) blends did not change significantly after adding TiO_2 nanoparticles. The phase structure of PLA/PCL/TiO_2 composites prepared with various mixing protocols did not differ remarkably from each other. The size distribution of PCL inclusions in all composites remained approximately the same. However, the toughness measurements are extremely sensitive even on subtle structure changes and inhomogeneities.

The notched impact strength of all PLA/PCL/TiO_2 composites with 5 and 10 wt.% of TiO_2 (Table 1) was measured and compared with that of PLA/PCL (80/20) blend (Fig. 9). All PLA/PCL/TiO_2 composites exhibited lower toughness than the PLA/PCL (80/20) blend. The decrease was correlated with TiO_2 concentration. The way of sample preparation had a significant impact on the composite with 10 wt.% of TiO_2; the highest impact strength was noticed for composite prepared by simultaneous mixing of all components (sample 72/18/10/a), but still the toughness was reduced to 52 % in comparison with the original blend PLA/PCL (80/20). For composite with 5 wt.% of TiO_2 (sample 76/19/5/a) we got 66% of PLA/PCL (80/20) blend value.

The stiffness of all composites increased slightly with respect to the neat blend (Fig. 10). The sample preparation influence on the composite stiffness was negligible. The stiffness increased about 6 % and 11 % with 5 and 10 wt.% of TiO_2 content, respectively. Generally, the addition of TiO_2 could be used to fine-tune the toughness and stiffness of PLA/PCL blends, as illustrated in Figs. 3, 9 and 10. The effect of the TiO_2

particles on the stiffness was somewhat smaller than predicted by the Einstein equation for non-interacting particles well adhering to the matrix,[51] which indicated that the adhesion between PLA and TiO_2 was not perfect. The weak effect of TiO_2 on the blend stiffness also confirmed, in agreement with the morphology observed in Fig. 8, that the TiO_2 nanoparticles tended to form small distinct aggregates rather than a stiffening physical network. In any case, the expected increase in stiffness due to TiO_2 nanoparticles showed to be quite modest and the impact on toughness was negative. We conclude that the best combination of mechanical properties can be achieved by optimizing PLA/PCL ratio without the addition of TiO_2.

3.2.3 Micromechanical properties of PLA/PCL/TiO_2 composites

Micromechanical measurements of PLA/PCL/TiO_2 composites (Fig. 11) confirmed the results of DMA (Fig. 10). The addition of TiO_2 just slightly increased stiffness of the system, as evidenced by indentation modulus, E_{IT} (Fig. 11, dark-gray columns). This small increase corresponded to the trend observed for shear modulus (compare Fig. 10 and 11) and was in agreement with theory (Eq. 4 and 8). Microindentation hardness, H_{IT} (Fig. 11, light-gray columns) followed more-or-less the same trend as E_{IT}. The justification of this behavior is connected with the works of Struik,[52] Flores et al.[53] and Balta-Calleja et al.[38] Struik[52] developed a model which relates yield stress (σ_Y) of polymers to the tensile elastic modulus (E):

$$\sigma_Y \approx E/30. \quad (9)$$

The model represented by Eq. 9 was successfully tested for various amorphous and semicrystalline polymers.[38,53] If we consider Eq. 4, the combination of Eq. 7 and 9 gives the approximate relation between microhardness (H_{IT}) and tensile modulus (E_{IT}), valid for semicrystalline polymers:

$$H_{IT} \approx 3\sigma_Y \approx E_{IT}/10. \quad (10)$$

According to Eq. 10, our systems containing ca 80% of semicrystalline PLA matrix should give approximate ratio $E_{IT}/H_{IT} \approx 10$. The actual average E_{IT}/H_{IT} ratio of all composites in Fig. 11 ranged from 15 to 17. The E_{IT}/H_{IT} ratio for all PLA/PCL blends (section 3.1) was in the same range. This was in reasonable agreement with theory and confirmed the consistency of our measurements. In conclusion, the microindentation hardness measurements re-confirmed the very good agreement between micro- and macromechanical properties (section 3.1.3) and the fact that the addition of TiO_2 did not bring any important benefit (section 3.2.2) for mechanical properties.

4. Conclusion

The objective of this study was to prepare PLA/PCL blends with a well-balanced combination of stiffness and toughness. The basic idea was using PCL as an impact modifier and achieving the best properties by careful optimization of composition, processing and phase morphology. Due to the biocompatibility and biodegradability of both polymers, PLA/PCL blends would be suitable for numerous biomedical, packaging and agricultural applications.

We have demonstrated that proper choice of the components (PLA/PCL viscosity ratio ~1/1; Fig. 1) combined with specific processing conditions (melt-mixing followed by compression molding combined with fast cooling), resulted in optimal morphology (PLA matrix containing small PCL particles) and synergistic improvement of toughness at the expense of moderate decrease in stiffness. We have also tested addition of biocompatible filler – TiO_2 nanoparticles – to the blend with optimized composition. Morphology of the blends and composites was characterized by electron microscopy and DSC. Toughness was assessed by means of Charpy impact testing and stiffness was obtained from DMA experiments. Microindentation hardness testing yielded the values of indentation modulus and hardness. The results of macro- and micromechanical measurements were compared with each other and with the predictive theory based on Equivalent Box Model (EBM). The main results are summarized below:

1. Toughness of the prepared PLA/PCL blends (Fig. 2) achieved local maximum at the composition 80/20, where it was 16 times higher in comparison with pure PLA, exceeding even the impact strength of pure impact modifier, PCL (Fig. 3). This was a clear synergistic effect, achieved partially due to the careful optimization of the blend preparation and partially due to serendipity in combining all favorable factors such as phase morphology of the blend and crystallinities of both components.
2. Stiffness of the PLA/PCL blends inevitably decreased with increasing concentration of soft PCL component. However, the decrease was mild, lower than predicted by EBM theory (Fig. 4). In other words, the high stiffness of the PLA matrix was not influenced adversely by the impact modifier particles.
3. The moduli from microindentation hardness testing were in excellent agreement with the macroscopic moduli from DMA experiments (Fig. 5). The results from micromechanical testing confirmed that the decrease in stiffness, observed at macroscopic scale, was better than predicted from the properties of the individual components. Both indentation modulus and indentation hardness showed positive deviations from EBM model, which indicated formation of very strong interfacial layer and synergistic improvements of mechanical properties (Figs. 6 and 7).
4. The addition of TiO_2 nanoparticles (5 and 10 wt.%) did not affect the morphology of PLA/PCL (80/20) blend significantly (Fig. 8). It caused substantial decrease in the impact strength (Fig. 9), but only slight improvement of stiffness (Fig. 10), as confirmed by micromechanical testing (Fig. 11). Although the impact strength of PLA/PCL/TiO_2 composites remained several times higher in comparison with pure PLA, we concluded that the addition of TiO_2 did not bring any apparent benefit to mechanical properties.

Acknowledgments: Financial support from the Czech Science Foundation (Grant No. GA14-17921S) is gratefully

acknowledged. The work at the Institute of Macromolecular Chemistry was also supported by the Ministry of Education, Youth and Sports of the Czech Republic within the National Sustainability Program I (NPU I), project POLYMAT LO1507.

5. References

1. V. Mourino, *J. R. Soc. Interface*, 2010, **7**, 209-227.

2. J. C. Middleton, *Biomaterials*, 2000, **21**, 2335-2346.

3. J. R. Porter, T. T. Ruckh and K. C Popat, *Biotechnol Prog.*, 2009, **6**, 1539-1560.

4. C. B. Bucknall. *Toughened plastics*, Applied Science Publishers, London, 1977.

5. E. Can, G. Udenir, A. I. Kanneci, G. Kose and S. Bucak, *AAPS PharmSciTech*, 2011, **12**, 1442-1453.

6. T. Patrício, A. Glória and P. Bártolo, *Chem. Eng. Trans.*, 2012, **32**, 1645-1650.

7. M. Todo, S-D. Park, T. Takayama and K. Arakawa, *Eng. Frac. Mech.*, 2007, 74, 1872-1883.

8. L. Cabedo, J. L. Feijoo, M. P. Villanueva, J. M. Lagarón and E. Giménez, *Macromol. Symp.*, 2006, **233**, 191-197.

9. N. López-Rodríguez, A. López-Arraiza, E. Meaurio and J. R. Sarasua, *Polym. Eng*. *Sci.*, 2006, **46**, 1299-1308.

10. V. Vilay, M. Mariatti, Z. Ahmad, K. Pasomsouk and M. Todo, *J. Appl. Polym. Sci.*, 2009, **114**, 1784-1792.

11. V. Mittal, T. Akhatar, G. Luckachan and N. Matsko, *Colloid Polym. Sci.*, 2015, **293**, 573-585.

12. V. Mittal, T. Akhatar and N. Matsko, *Macromol. Mater. Eng.*, 2015, **300**, 423-435.

13. H. Bai, C. Huang, H. Xiu, Y. Gao, Q. Zhang and Q. Fu, *Polymer*, 2013, **54**, 5257-5266.

14. J. Urquijo, G. Guerrica-Echavarria and J. I. Equiazabal, *J. Appl. Polym. Sci.*, 2015, **132**, 42641

15. B. Imre and B. Pukánszky, *Eur. Polym. J.*, 2013, **49**, 1215-1233.

16. D. Wu, Y. Zhang, L. Yuan, M. Zhang and W. Zhou, *J. Polym. Sci. Pt. B-Polym. Phys.*, 2010, **48**, 756-765.

17. O. Monticelli, M. Calabrese, L. Gardella, A. Fina and E. Gioffredi, *Eur. Polym. J.*, 2014, **58**, 69-78.

18. R. Dell'Erba, G. Groenickx, G. Maglio, M. Malinconico and A. Migliozzi, *Polymer*, 2001, **42**, 7831-7840.

19. L. Gardella, M. Calabrese and O. Monticelli, *Colloid Polym. Sci.*, 2014, **292**, 2391-2398.

20. V. B. Carmona, A. C. Corrêa, J. M. Marconcini and L. H. C. Mattoso, *J. Polym. Environ.*, 2015, **23**, 83-89.

21. T. Takayama, M. Todo and H. Tsuji, *J. Mech. Behav. Biomed. Mater.*, 2011, **4**, 255-260.

22. I. Fortelný, A. Ostafińska, D. Michálková, J. Jůza, J. Mikešová and M. Šlouf, *Polym. Bull.*, *2015*, **72**, 2931-2947

23. T. Kasuga, H. Kondo and M. Nogami, *J. Cryst. Growth*, 2002, **235**, 235-240.

24. N. A. Ali and F. T. M. Noori, *Chem. Mat. Res.* 2014, **4**, 44.

25. J. Mikesova, M. Slouf, U. Gohs, D. Popelkova, T. Vackova, N. H. Vu, J. Kratochvil and A. Zhigunov, *Polym. Bull.*, 2014, **71**, 795–818.

26. N. Nakayama and T. Hayashi, *Polym. Degrad. Stabil.*, 2007, **92**, 1255-1264.

27. J. Kolarik, *Polym. Eng. Sci.*, 1996, **36**, 2518–2524.

28. M. Šlouf, A. Ostafińska, M. Nevoralová and I. Fortelný, *Polym. Test.*, 2015, **42**, 8-16.

29. M. Šlouf, J. Kolařík, and J. Kotek, *Polym. Eng. Sci.*, 2007, **47**, 582-592.

30. Q. Guo and G. Groeninckx, *Polymer*, 2001, **42**, 8647-8699.

31. J. F. Turner, A. Riga, A. O'Connor, J. Zhang and J. Collis, *Therm. Anal. Calorim.*, 2004, **75**, 257-268.

32. F. J. Balta-Calleja and S. Fakirov, *Microhardness of Polymers*, first ed., Cambridge University Press, 2000.

33. M. Slouf, T. Vackova, M. Nevoralova and D. Pokorny, *Polym. Test*, 2015, **41**, 191–197.

34. W. C. Oliver and G. M. Pharr, *J. Mater. Res.*, 1992, **7**, 1564–1583.

35. T. Vackova, M. Slouf, M. Nevoralova and L. Kapralkova, *Eur. Polym. J.*, 2012, **48**, 2031–2039.

36. M. Slouf, J. Kolarik and J. Kotek, *Polym. Eng. Sci.*, 2007, **47**, 582-592.

37. D. Tabor, The hardness of metals. Oxford University Press, New York (1951).

38. F. J. Balta-Calleja and S. Fakirov, *Microhardness of Polymers*, first ed., Cambridge University Press, 2000, Chapter 4: Microhardness of crystalline polymers, pages 80–126.

39. J. Odent, J.-M. Raquez, E. Duquesne and P. Dubois, *Eur. Polym. J.*, 2012, **48**, 331-340.

40. G. Perego, G. D. Cella and C. Bastioli, *J. Appl. Polym. Sci.*, 1996, **59**, 37–43.

41. J. Odent, J.-M. Raquez, P. Leclère, F. Lauro and P. Dubois, *Polym. Adv. Technol.*, 2015, **26**, 814-822.

42. C. B. Bucknall and D. R. Paul, *Polymer*, 2013, **54**, 320-329

43. C. B. Bucknall, Deformation Mechanisms in Rubber-Toughened Polymers. In: C. B. Bucknall and D. R. Paul (eds), Polymer Blends, V. 2: Performance, John Wiley & Sons, 2000.

44. R. J. Gaymans, Toughening Semicrystaline Thermoplastics. In: C. B. Bucknall and D. R. Paul (eds.), Polymer Blends, V. 2: Performance, John Wiley & Sons, 2000.

45. A. C. Renouf-Glauser, J. Rose, D. F. Farrar and R. E. Cameron, *Biomaterials*, 2005, **26**, 5771-5782.

46. H. Bai, H. Xiu, J. Gao, H. Deng, Q. Zhang, M. Yang and Q. Fu, *ACS Appl. Mater. Interfaces*, 2012, **4**, 897-905.

47. H. F. Brinson and L. C. Brinson, Polymer engineering Science and Viscoelasticity: An Introduction. Chapter: Stress and Strain Analysis and Measurement, 2008.

48. N. G. McCrum, C. P. Buckley and C. B. Bucknall: Principles of Polymer Engineering, Chapter: Reinforced polymers. Oxford University press, 2nd ed., 2003.

49. J. Kolarik, *J. Macromol. Sci. Part B-Phys.*, 2000, **39**, 53–66.

50. J. P. Mofokeng and A. S. Luyt, *Polym. Test.*, 2015, **45**, 93-100.

51. E. D. Bliznakov, C. C. White and M. T. Shaw, *J. Appl. Polym. Sci.,* 2000, **77**, 3220–3227.

52. L. C. E. Struik, *J. Non-Cryst. Solids*, 1991, **131**, 395-407.

53. A. Flores, F. J. Balta Calleja, G. E. Attenburrow and D. C. Basset, *Polymer*, 2000, **41**, 5431–5435.

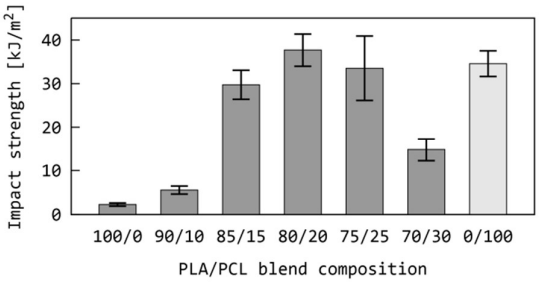

Blending of poly(lactic acid) with poly(ϵ-caprolactone) can increase the impact strength above the values of the individual components.